Extracting trajectory equations of classical periodic orbits from the quantum eigenmodes in two-dimensional integrable billiards

Y. H. Hsieh, Y. T. Yu, P. H. Tuan, J. C. Tung, K. F. Huang, and Y. F. Chen
Department of Electrophysics, National Chiao Tung University, 1001 Ta-Hsueh Road, Hsinchu 30010, Taiwan
(Received 10 August 2016; revised manuscript received 24 January 2017; published 21 February 2017)

The trajectory equations for classical periodic orbits in the equilateral-triangular and circular billiards are systematically extracted from quantum stationary coherent states. The relationship between the phase factors of quantum stationary coherent states and the initial positions of classical periodic orbits is analytically derived. In addition, the stationary coherent states with noncoprime parametric numbers are shown to correspond to the multiple periodic orbits, which cannot be explicable in the one-particle picture. The stationary coherent states are further verified to be linked to the resonant modes that are generally observed in the experimental wave system excited by a localized and unidirectional source. The excellent agreement between the resonant modes and the stationary coherent states not only manifests the importance of classical features in experimental systems but also paves the way to manipulate the mesoscopic wave functions localized on the periodic orbits for applications.

DOI: 10.1103/PhysRevE.95.022214

I. INTRODUCTION

Since Schrödinger first constructed the coherent state for the one-dimensional harmonic oscillator to mimic the classical dynamics [1,2], the coherent superposition has been identified to play an important role in the quantum-classical connection. Extending Schrödinger's method to the two-dimensional (2D) harmonic oscillator, the stationary coherent states superposed by a group of degenerate eigenstates have been derived to demonstrate that their wave patterns can be exactly localized on the classical periodic orbits (POs), i.e., Lissajous figures [3]. In addition to harmonic oscillators, the 2D billiard systems widely serve as the paradigm for exploring the quantum-classical correspondence, since they can be simply employed to analyze a variety of dynamical features by changing geometric shapes [4–12]. So far, most investigations on billiard systems have mainly focused on nonintegrable and irregular shapes [12–21]. One of the intriguing findings in nonintegrable billiards is the emergence of eigenstates localized on the unstable POs. Even so, the number of eigenstates related to unstable POs is rather few. The eigenstates in nonintegrable billiards for the most part are extensively distributed in the coordinate spaces [14,21] and usually display a common feature of quasi-linear-ridge structures [21,22].

In contrast to nonintegrable billiards, stable POs are generally abundant in integrable billiards with symmetric shapes [4,17,23–38]. The quantum wave functions related to the stable POs have been verified to play a critical role in numerous striking physics including conductance fluctuations [39], ballistic transport [40,41], and directional emissions [42–57]. It has been confirmed that quantum coherent states constructed by the coherent superposition of nearly degenerate eigenstates can manifest the wave functions to be associated with the classical POs in integrable billiards [5,6]. Quantum wave functions related to classical POs with different initial positions can be utterly obtained by changing the phase factor and the central order in the constructed stationary coherent states. Nevertheless, trajectory equations for classical POs have not been completely extracted from quantum stationary coherent states until now. A thorough extraction for trajectory equations from quantum coherent states is pedagogically important in understanding the quantum-classical connection.

In this work, a theoretical approach for constructing quantum stationary coherent states to manifest classical POs is systematically reviewed in integrable billiards, including the equilateral-triangular and circular shapes. In terms of the central order (m_0,n_0) and the phase factor ϕ_0, the wave representation of stationary coherent states is employed to extract trajectory equations analytically for the classical POs. The extracted trajectory equations clearly reveal the relationship between the parameters (m_0,n_0,ϕ_0) of the stationary coherent states and the initial position (x_0,y_0) of the classical POs described by the indices (p,q). Furthermore, we analyze the stationary coherent states for the noncoprime indices (p,q) and show the wave patterns to be localized on the multiple POs. The feature of quantum wave patterns related to multiple POs has no correspondence in the one-particle picture. Finally, we verify that the stationary coherent states can be linked to the resonant modes generally observed in the experimental wave system excited by a localized and unidirectional source [58,59]. The good agreement between the stationary coherent states and the experimental resonant modes sheds light on using the present model to manipulate the generation of quantum wave functions related to classical POs for feasible applications.

II. EXTRACTING TRAJECTORY EQUATIONS FOR EQUILATERAL TRIANGULAR BILLIARDS

We first consider equilateral-triangular billiards to demonstrate the approach for extracting the trajectory equations for classical POs from quantum stationary coherent states. For an equilateral-triangular billiards with three vertices at $(0,0)$, $(a/2,\sqrt{3}a/2)$, and $(-a/2,\sqrt{3}a/2)$, the eigenvalues and eigenfunctions are given by [60]

$$E_{m,n} = (m^2 + n^2 - mn)\varepsilon_0 \tag{1}$$

*Corresponding author: yfchen@cc.nctu.edu.tw

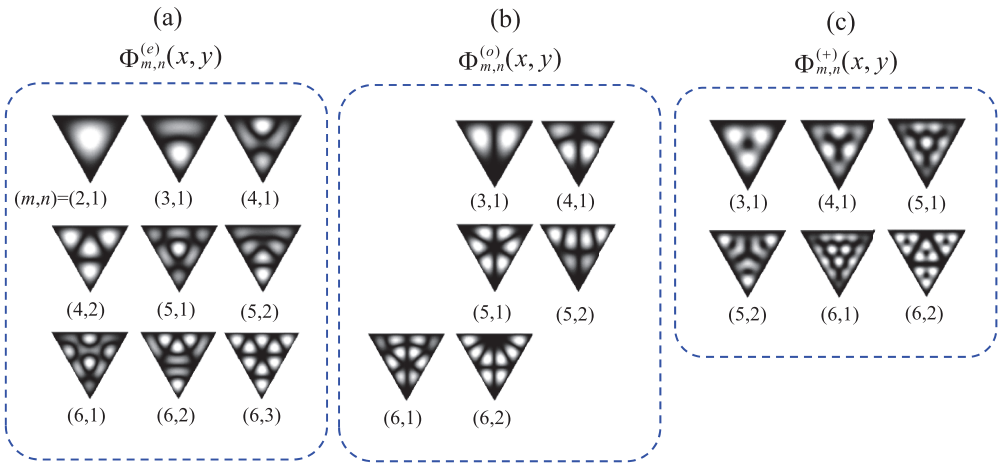

FIG. 1. Wave patterns of (a) $|\Phi^{(e)}_{m,n}(x,y)|$, (b)$|\Phi^{(o)}_{m,n}(x,y)|$, and (c) $|\Phi^{(+)}_{m,n}(x,y)|$ for several sets of quantum numbers (m,n).

and

$$\Phi^{(o)}_{m,n}(x,y), \Phi^{(e)}_{m,n}(x,y) = \sqrt{\frac{16}{a^2 3\sqrt{3}}} \left\{ \begin{matrix} \sin \\ \cos \end{matrix} \left[\frac{2\pi}{3a}(2m-n)x \right] \sin\left(\frac{2\pi}{\sqrt{3}a} ny \right) - \begin{matrix} \sin \\ \cos \end{matrix} \left[\frac{2\pi}{3a}(2n-m)x \right] \sin\left(\frac{2\pi}{\sqrt{3}a} my \right) + \begin{matrix} \sin \\ \cos \end{matrix} \left[-\frac{2\pi}{3a}(m+n)x \right] \sin\left[\frac{2\pi}{\sqrt{3}a}(m-n)y \right] \right\}, \quad (2)$$

where $\varepsilon_0 = 9\hbar^2\pi^2/8\mu a^2$ is the unit energy of the equilateral-triangular billiards, $\hbar$ is the reduced Planck's constant, and μ is the mass of particle. Here the quantum numbers m and n are non-negative integers and the superscripts (o) and (e) denote the two types of degenerate modes with odd and even symmetries, respectively. The form of $\Phi^{(e)}_{m,n}(x,y)$ and $\Phi^{(o)}_{m,n}(x,y)$ in Eq. (2) is the standing-wave representation. It is necessary to use the traveling-wave representation for constructing the stationary coherent states related to the classical POs. In terms of $\Phi^{(e)}_{m,n}(x,y)$ and $\Phi^{(o)}_{m,n}(x,y)$, the traveling-wave representation is given by $\Phi^{(\pm)}_{m,n}(x,y) = \Phi^{(e)}_{m,n}(x,y) \pm i\Phi^{(o)}_{m,n}(x,y)$, where the superscripts $(+)$ and $(-)$ denote the forward and backward traveling states, respectively. Figures 1(a)–1(c) show the intensity wave patterns of $\Phi^{(e)}_{m,n}(x,y)$, $\Phi^{(o)}_{m,n}(x,y)$, and $\Phi^{(+)}_{m,n}(x,y)$ with different sets of quantum numbers (m,n), respectively. Since the wave patterns for $|\Phi^{(+)}_{m,n}(x,y)|$ and $|\Phi^{(-)}_{m,n}(x,y)|$ are similar in spatial morphologies, only the case of $|\Phi^{(+)}_{m,n}(x,y)|$ is shown in Fig. 1(c). The intensity patterns for all cases can be seen to be symmetric with respect to the y axis due to the setting of the equilateral triangle.

The quantum stationary coherent states related to the classical POs are formed by the superposition of the nearly degenerate eigenstates [5,6,9]. The nearly degenerate condition for the integrable billiards with the central order (m_0,n_0) can be derived from the tangent of the constant-energy contour with the slope given by

$$-\left.\frac{dn}{dm}\right|_{m_0,n_0} = \frac{\partial E/\partial m|_{m_0,n_0}}{\partial E/\partial n|_{m_0,n_0}} = \frac{2m_0 - n_0}{2n_0 - m_0}, \quad (3)$$

as shown in Fig. 2 for the spectrum of eigenvalues. Each gray point in the spectrum of Fig. 2 represents an eigenstate denoted by (m,n) and the solid black line marks the constant-energy contour with the central order (m_0,n_0). If the slope in Eq. (3) is given by a rational number q/p, the central eigenstate for the coherent superposition can be written as $m_0 = (2q+p)N$ and $n_0 = (2p+q)N$ with a single parameter N to determine the mode order. The rational slope q/p is used to make a connection with classical POs for convenience. In terms of the indices (p,q), the coherent superposition of $2M+1$ nearly degenerate eigenstates around the central mode of (m_0,n_0) can be

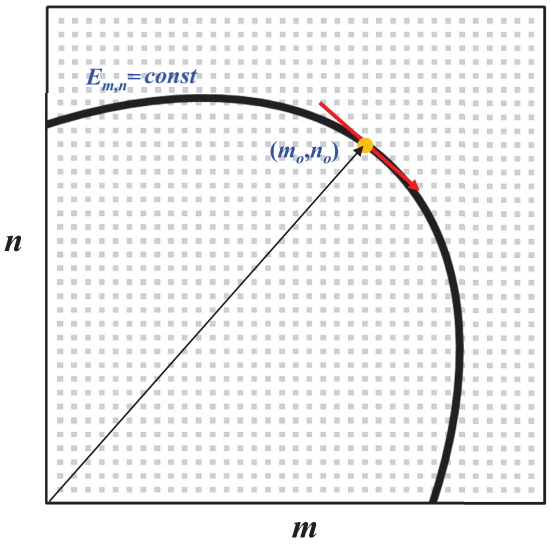

FIG. 2. Spectrum of eigenvalues in the equilateral triangular billiards. Each gray point represents an eigenstate denoted by (m,n) and the solid black line marks the constant-energy contour with central order to be (m_0,n_0).

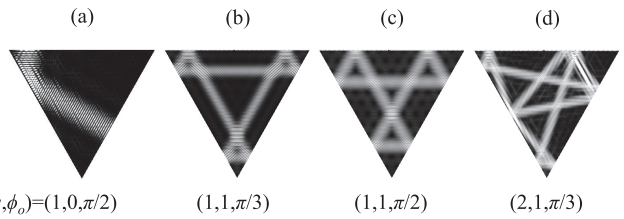

FIG. 3. Wave patterns of $|\Psi^{(+)}_{N,M}|$ calculated by Eq. (4) with $N = 30, M = 5$, and different sets of (p,q,ϕ_0): (a) $(1,0,\pi/2)$, (b) $(1,1,\pi/3)$, (c) $(1,1,\pi/2)$, and (d) $(2,1,\pi/3)$.

given by

$$\Psi^{(\pm)}_{N,M}(x,y;p,q,\phi_0) = \frac{1}{\sqrt{2M+1}} \sum_{K=-M}^{M} e^{iK\phi_0} \Phi^{(\pm)}_{m_0+pK,n_0-qK}(x,y), \quad (4)$$

where ϕ_0 is the phase factor in the range $-\pi \leqslant \phi_0 \leqslant \pi$. As discussed later, the phase factor ϕ_0 is related to the initial position of the classical PO. From Eq. (1) it can be found that the eigenenergies of the superposed eigenstates are nearly a constant energy of $E_{SC} = E_{m_0,n_0} + 3pqNM\varepsilon_0$ under the conditions $m_0 \gg pM$ and $n_0 \gg qM$. Since $\Psi^{(+)}_{N,M}$ and $\Psi^{(-)}_{N,M}$ form a conjugate pair with identical spatial patterns, only the traveling state $\Psi^{(+)}_{N,M}$ is presented in the following. Figures 3(a)–3(d) show the wave patterns of $|\Psi^{(+)}_{N,M}|^2$ calculated by Eq. (4) with $N = 30, M = 5$, and different sets of (p,q,ϕ_0). Here the indices (p,q) are coprime. The result for the noncoprime (p,q) will be discussed later in this section. The wave patterns of stationary coherent states given by Eq. (4) can be seen to be well localized on the classical POs. The velocity direction of the trajectory can be straightforwardly determined by the slope q/p.

Since the stationary coherent states can perfectly manifest the morphologies of classical POs, they can be employed to extract the trajectory equations for POs by means of determining the central maximum of the wave intensity. Using Euler's formula $\exp(i\theta) = \cos\theta + i\sin\theta$ to express the sine and cosine functions in Eq. (2), after some algebra, the stationary coherent states can be further simplified as

$$\begin{aligned}\Psi^{(+)}_{N,M}(x,y;p,q,\phi_0) = &\left\{\exp\left[-i\left(\frac{2(m_0+n_0)\pi}{3a}x \mp \frac{2\pi(m_0-n_0)}{\sqrt{3}a}y\right)\right] D_M\left(\frac{2\pi}{3a}[(p-q)x \mp \sqrt{3}(p+q)y + \phi_0]\right)\right.\\ &\pm \exp\left[-i\left(\frac{2(2m_0+n_0)\pi}{3a}x \mp \frac{2\pi n_0}{\sqrt{3}a}y\right)\right] D_M\left(\frac{2\pi}{3a}[(2p+q)x \mp \sqrt{3}qy + \phi_0]\right)\\ &\left.\mp \exp\left[-i\left(\frac{2(2n_0+m_0)\pi}{3a}x \mp \frac{2\pi m_0}{\sqrt{3}a}y\right)\right] D_M\left(\frac{2\pi}{3a}[(p+2q)x \mp \sqrt{3}py + \phi_0]\right)\right\}, \quad (5)\end{aligned}$$

where $D_M(\theta) = (2i\sqrt{2M+1})^{-1}\sum_{K=-M}^{M} e^{iK\theta}$ is the Dirichlet kernel that has the maxima at $\theta = 2n\pi$ for any integer n. Using the maximal feature of the Dirichlet kernel, the parametric equations for the central maxima of $|\Psi^{(+)}_{N,M}|$ can be deduced as

$$A_s x + B_s y + \phi_0 = 2n\pi, \quad (6)$$

where $-A_s/B_s = \eta_s$ are the slopes for line equations with $s = 1,2,\ldots,6$. The family of Eq. (6) is exactly related to the trajectory equations for the classical POs. From Eq. (5) the slopes for all trajectories can be found to be $\eta_1 = -\eta_2 = (p-q)/\sqrt{3}(p+q)$, $\eta_3 = -\eta_4 = (p+2q)/\sqrt{3}p$, and $\eta_5 = -\eta_6 = (2p+q)/\sqrt{3}q$. Equation (6) clearly indicates that the classical POs of the equilateral-triangular billiards are constituted by six independent line equations with different slopes. The initial position (x_0,y_0) and the velocity (v_x,v_y) in classical dynamics are linked to Eq. (6) by the identities $A_s x_0 + B_s y_0 = 2n\pi - \phi_0$ and $v_y/v_x = (dy/dt)/(dx/dt)|_{x_0,y_0} = \eta_s$. In other words, the phase factor ϕ_0 of the stationary coherent state is directly related to the initial position (x_0,y_0). On the other hand, the velocity (v_x,v_y) in classical dynamics depends only on the parameters p and q. Figure 4 shows the correspondence between the classical POs by the trajectory equations with $(x_0,y_0) = (0.05a,0.52a)$ and their quantum counterparts of stationary coherent states calculated under different parameters of (s,p,q). The black points mark the initial positions and the black arrows denote the velocities of the classical particle. The good agreement between the classical trajectory patterns and the quantum wave patterns confirms that the trajectory equations for the classical POs can be perfectly extracted from the quantum stationary coherent states.

Before concluding this section, we turn to the case of noncoprime (p,q). The greatest common divisor for noncoprime (p,q) is denoted by l. By using the identity $(l)^{-1}\sum_{s=0}^{l-1} e^{i2\pi us/l} = \delta_{u,lM}$ for any integer u and $M = 0,\pm1,\pm2,\ldots$, the stationary coherent state in Eq. (4) can be

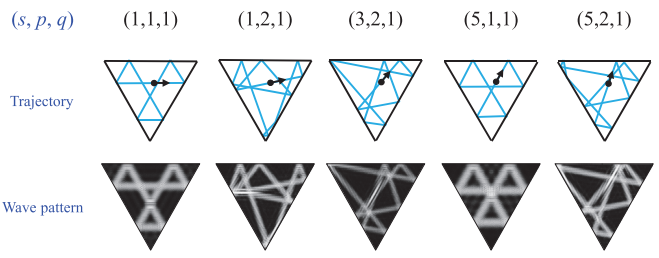

FIG. 4. Correspondence between the classical POs by the trajectory equations with $(x_0,y_0) = (0.05a,0.52a)$ and their quantum counterparts of stationary coherent states calculated with different parameters of (s,p,q).

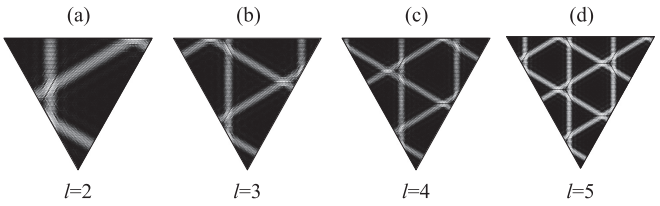

FIG. 5. Wave patterns of the stationary coherent states given by Eq. (7) with the parameters $N = 30, M = 5, (p/l,q/l) = (1,0), \phi_0 = 0.5\pi$, and (a) $l = 2$, (b) $l = 3$, (c) $l = 4$, and (d) $l = 5$.

rewritten in a form with double summation

$$\Psi^{(\pm)}_{N,M}(x,y;p,q,\phi_0) = \frac{1}{l\sqrt{2M+1}} \sum_{s=0}^{l-1} \sum_{u=-lM}^{lM} e^{iu\phi_{l,s}} \Phi^{(\pm)}_{m_0+(pu/l),n_0-(qu/l)}(x,y), \tag{7}$$

where $\phi_{l,s} = (\phi_0 + 2\pi s)/l$. Note that the running index K in Eq. (4) has been changed as s and u. Equation (7) indicates that the stationary coherent state for the noncoprime (p,q) can be expressed as the sum of l stationary coherent states with coprime indices $(p/l,q/l)$ and the phase factors $\phi_{l,s}$. Figures 5(a)–5(d) present the wave patterns of the stationary coherent states in Eq. (7) with the parameters $N = 30$, $M = 5$, $(p/l,q/l) = (1,0)$, $\phi_0 = 0.5\pi$, and $l = 2,3,4,5$, respectively. It can be clearly seen that the wave patterns of stationary coherent states are simultaneously localized on l classical POs with the initial positions determined by the phase factors $\phi_{l,s}$. It is worth noting that there is no correspondence in the one-particle picture for the quantum wave patterns localized on the multiple POs.

III. EXTRACTING TRAJECTORY EQUATIONS FOR CIRCULAR BILLIARDS

The circular billiards is analyzed to further confirm the present approach of extracting the trajectory equations for classical POs from quantum stationary coherent states. The eigenvalues and the eigenfunctions in polar coordinates for a circular billiards with a radius R are given by

$$E_{m,n} = \frac{\hbar^2}{2\mu} k^2_{m,n} \tag{8}$$

and

$$\Phi_{m,n}(r,\theta) = \frac{1}{\sqrt{\pi}\, R J_{m-1}(k_{m,n}R)} J_m(k_{m,n}r) e^{im\theta}, \tag{9}$$

where $k_{m,n} = \alpha_{m,n}/R$ and $\alpha_{m,n}$ is the nth zero of the first kind of Bessel function $J_m(z)$ with order m. Figure 6(a) depicts the wave patterns of $\Phi_{m,n}(r,\theta)$ with different quantum numbers (m,n). It is clear that the indices n and m are related to the nodal structures in the radial and azimuthal directions, respectively. To determine the nearly degenerate condition for the circular billiards, the Wentzel-Kramers-Brillouin (WKB) method is employed to derive the analytical form for the eigenvalues

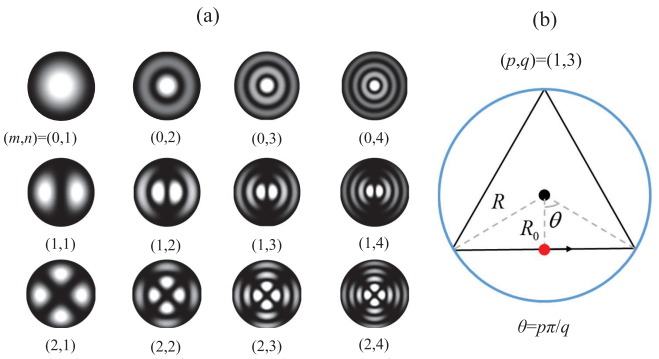

FIG. 6. (a) Wave patterns of $|\Phi_{m,n}(r,\theta)|$ with different quantum numbers (m,n). (b) Schematic diagram of the classical PO defined as $(p,q) = (1,3)$ in circular billiards.

$k_{m,n}$ as

$$\sqrt{k^2_{m,n}(R^2 - R_0^2)} - m\cos^{-1}\left(\frac{R_0}{R}\right) = \left(n + \frac{3}{4}\right)\pi, \tag{10}$$

where $R_0 = R\cos(p\pi/q)$ is the shortest distance to the circular center for the periodic orbits (p,q), as shown in Fig. 6(b). Here q is the number of turning points at the boundary during one period and p is the number of windings during one period. From the correspondence of the orbital angular momentum, another quantum-classical connection can be obtained as $L_z = m\hbar = R_0\hbar k_{m,n}$. Substituting the relation $m = R_0 k_{m,n}$ into Eq. (10), the WKB quantization can be simplified as $k_{m,n}R\sin(p\pi/q) = [m(p/q) + n + (3/4)]\pi$. Under the condition $m_0 \gg |qK|$, it can be found that the group of eigenstates Φ_{m_0+qK,n_0-pK} with $K \in \mathbb{Z}$ constitutes a family of nearly degenerate states and their eigenvalues form an energy shell in the neighborhood of the central state Φ_{m_0,n_0}. In terms of the nearly degenerate eigenstates Φ_{m_0+qK,n_0-pK} and the phase factor ϕ_0, the stationary coherent states for the circular billiards can be given by

$$\Psi_{m_0,M}(r,\theta;p,q,\phi_0) = \frac{1}{\sqrt{2M+1}} \sum_{K=-M}^{M} e^{iKq\phi_0} \Phi_{m_0+qK,n_0-pK}(r,\theta). \tag{11}$$

Figures 7(a)–7(d) show the wave patterns $|\Psi_{m_0,M}|$ calculated with $m_0 = 300, M = 2$, and different sets of parameters (p,q,ϕ_0). All the wave patterns can be seen to be well localized on the classical POs of the circular billiards. Furthermore, the wave patterns near the periphery of the billiards can be found

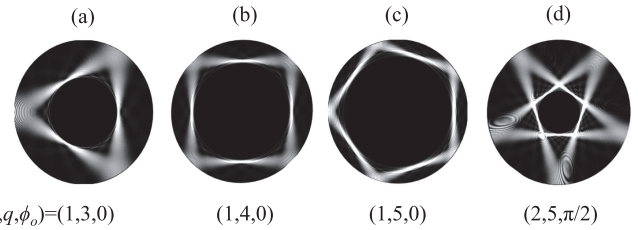

FIG. 7. Wave patterns $|\Psi_{m_0,M}(r,\theta;p,q,\phi_0)|$ calculated with $m_0 = 300, M = 2$, and different sets of parameters (p,q,ϕ_0): (a) (1,3,0), (b) (1,4,0), (c) (1,5,0), and (d) $(2,5,\pi/2)$.

to exhibit the ripple morphologies that are the characteristics arising from the interference of Bessel functions.

To extract the trajectory equations from the central maxima of the stationary coherent states, it is necessary to use the asymptotic form and the boundary condition for the Bessel function. By using the boundary condition $J_m(k_{m,n}R)=0$ and the asymptotic form $J_m(z)\approx\sqrt{2/\pi z}\cos[z-(2m+1)\pi/4]$ for $z\to\infty$, the coefficient related to the normalization constant can be given by $J_{m-1}(k_{m,n}R)\approx\sqrt{2/\pi k_{m,n}R}$ for high-order modes. In terms of this coefficient, the high-order eigenfunctions $\Phi_{m,n}(r,\theta)$ can be expressed as $\Phi_{m,n}(r,\theta)=(\sqrt{k_{m,n}/2R}/2\pi)\int_{-\pi}^{\pi}e^{ik_{m,n}r\sin(\varphi)}e^{im(\theta-\varphi)}d\varphi$. Substituting this expression into Eq. (11), the stationary coherent states can be rewritten as

$$\Psi_{m_0,M}(r,\theta;p,q,\phi_0)=\sqrt{\frac{(2M+1)k_{m_0,n_0}}{8\pi^2R}}\left[\int_{-\pi}^{\pi}e^{ik_{m_0,n_0}r\sin(\alpha+\theta+\phi_0)}e^{-im_0(\alpha+\phi_0)}D_M(q\alpha)d\alpha\right], \tag{12}$$

where the Dirichlet kernel is given by $D_M(q\alpha)=(2M+1)^{-1}\sum_{K=-M}^{M}e^{-iKq\alpha}$ and the integration variable has been changed to $\alpha=\varphi-\theta-\phi_0$. Since $D_M(q\alpha)$ is a periodic pulse function with period $2\pi/q$, the integration of Eq. (12) on the circle angle can be divided into q segments with the integration interval between $-\pi/q$ and π/q. Consequently, Eq. (12) can be expressed as

$$\Psi_{m_0,M}(r,\theta;p,q,\phi_0)=C_{m_0,n_0}\sum_{s=0}^{q-1}\left\{\int_{-\pi/q}^{\pi/q}\exp\left[ik_{m_0,n_0}r\sin\left(\alpha+\theta+\phi_0-\frac{2\pi s}{q}\right)\right]\exp\left[-im_0\left(\alpha+\phi_0-\frac{2\pi s}{q}\right)\right]D_M(q\alpha)d\alpha\right\}, \tag{13}$$

where $C_{m_0,n_0}=\sqrt{(2M+1)k_{m_0,n_0}/8\pi^2R}$ is the normalization constant. For $(2M+1)q\gg1$, $D_M(q\alpha)$ displays a narrow peak concentrated in a small region of $-\Delta\leqslant\alpha\leqslant\Delta$ with $\Delta=\pi/q(2M+1)$. As a result, the factor $\sin(\alpha+\theta+\phi_0-2\pi s/q)$ in Eq. (13) can be expanded as $\alpha\cos(\phi_0+\theta-2\pi s/q)+\sin(\phi_0+\theta-2\pi s/q)$ under the small-angle approximation. To derive an analytical form, we further approximate $D_M(q\alpha)$ as a gate function whose values are unity in the interval $[-\Delta,\Delta]$ and vanish outside. By using these approximations and $k_{m_0,n_0}=m_0/R_0$, the integration in Eq. (13) can be performed as

$$\begin{aligned}\Psi_{m_0,M}(r,\theta;p,q,\phi_0)=&\sqrt{\frac{m_0}{2(2M+1)RR_0q^2}}e^{-im_0\phi_0}\\&\times\left(\sum_{s=0}^{q-1}\exp\left\{im_0\left[\frac{r}{R_0}\sin\left(\theta+\phi_0-\frac{2\pi s}{q}\right)+\frac{2\pi s}{q}\right]\right\}\operatorname{sinc}\left\{\frac{m_0}{R_0}\frac{\pi}{q(2M+1)}F_s(r,\theta,q)\right\}\right),\end{aligned} \tag{14}$$

where $\operatorname{sinc}(x)=\sin(x)/x$ is the sinc function and

$$F_s(r,\theta,q)=r\cos\left(\phi_0+\theta-\frac{2\pi s}{q}\right)-R_0, \tag{15}$$

with $s=0,1,\ldots,q-1$. Since the maximum of the function $\operatorname{sinc}(x)$ occurs at $x=0$, the trajectory equations for the classical POs determined by the central maxima of the stationary coherent states in Eq. (14) can be deduced as $F_s(r,\theta,q)=0$ with $s=0,1,\ldots,q-1$. Similar to the analysis for the equilateral-triangular billiards, the initial position (x_0,y_0) and the velocity (v_x,v_y) of the classical particle moving along the POs can be linked to the parameters (p,q,ϕ_0) by the expressions $R_0/\sqrt{x_0^2+y_0^2}=\cos(\phi_0+\theta-2\pi s/q)$ and $|v_yx_0-v_xy_0|/\sqrt{v_x^2+v_y^2}=R_0$. Figure 8 illustrates the correspondence between the classical POs evaluated by the trajectory equations with $(x_0,y_0)=(0.44a,0.31a)$ and the quantum counterparts of stationary coherent states calculated by using the related parameters of (p,q). The black points mark the initial positions and the black arrows denote the velocities of the classical particle. The good agreement between classical POs and quantum wave patterns once again confirms the present method of extracting the trajectory equations from the quantum stationary coherent states.

Similar to the analysis for the equilateral-triangular billiards, the case of noncoprime (p,q) is also considered for the circular billiards. Based on the same approach, the stationary coherent states in Eq. (11) for the noncoprime (p,q) with the greatest common divisor l can be rewritten as a double-summation form

$$\begin{aligned}&\Psi_{m_0,M}(r,\theta;p,q,\phi_0)\\&\quad=\frac{1}{l\sqrt{2M+1}}\sum_{s=0}^{l-1}\sum_{u=-lM}^{lM}e^{iu\phi_{l,s}}\Phi_{m_0+(qu/l),n_0-(pu/l)}(r,\theta),\end{aligned} \tag{16}$$

where $\phi_{l,s}=(q\phi_0+2\pi s)/l$. The wave patterns of the stationary coherent states calculated by Eq. (16) with the parameters $m_0=300, M=2$, $\phi_0=0$, and different sets of $(p/l,q/l)$

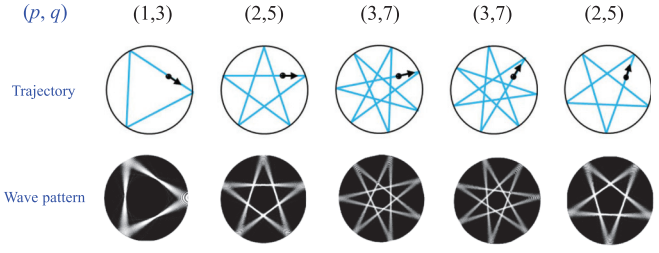

FIG. 8. Correspondence between the classical POs evaluated by the trajectory equations with $(x_0,y_0)=(0.44a,0.31a)$ and their quantum counterparts of stationary coherent states calculated under different parameters of (p,q).

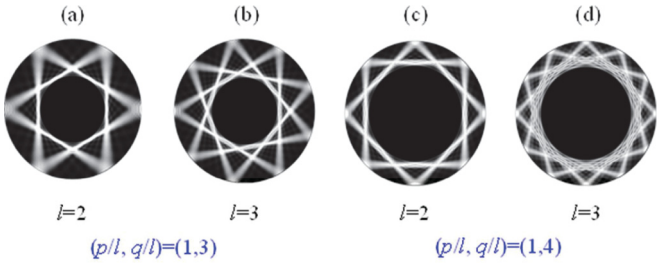

FIG. 9. Wave patterns of the stationary coherent states calculated by Eq. (16) with the parameters $m_0 = 300, M = 2$, $\phi_0 = 0$, and different sets of $(p/l,q/l)$ with (a) and (c) $l = 2$ and (b) and (d) $l = 3$.

with $l = 2,3$ are shown in Figs. 9(a)–9(d). It can be seen that the overall features for the noncoprime (p,q) in the circular billiards are the same as those obtained in the equilateral-triangular billiards.

IV. CONNECTION BETWEEN STATIONARY COHERENT STATES AND EXPERIMENTAL RESONANT MODES

It has been demonstrated that the trajectory equations for classical POs in integrable billiards can be exactly extracted from stationary coherent states. Next, we further verify that the stationary coherent states can be linked to the resonant modes that are generally observed in an experimental wave system excited by a localized and unidirectional source [58,59]. The connection between theoretical coherent states and experimental resonant modes can provide insight into the real mesoscopic systems.

For an experimental resonant system driven by an excitation source with the spatial distribution $S(x,y)$, the wave function of the stationary response $\tilde{\Psi}(x,y;\tilde{k})$ can be given by the inhomogeneous Helmholtz equation [59]

$$(\nabla^2 + \tilde{k}^2)\tilde{\Psi}(x,y;\tilde{k}) = S(x,y), \tag{17}$$

where the complex wave number $\tilde{k} = k + i\gamma$ is composed of the driving wave number k of the monochromatic source and the damping factor γ corresponding to the system dissipation. In terms of the eigenfunction expansion, the response wave function and the excitation source distribution can be respectively written as $\tilde{\Psi}(x,y;\tilde{k}) = \sum_n A_n(\tilde{k})\Phi_n(x,y)$ and $S(x,y) = \sum_n f_n\Phi_n(x,y)$, where $\Phi_n(x,y)$ are the eigenfunctions of the bound system. Substituting the results into Eq. (17), the comparison between the coefficients can lead to $A_n(\tilde{k}) = f_n/(\tilde{k}^2 - k_n^2)$, where k_n is the wave-number eigenvalue of the system. Note that here the equivalence of $\nabla^2\Phi_n(x,y) = -k_n^2\Phi_n(x,y)$ has been used. Hence the response wave function can be explicitly expressed as

$$\tilde{\Psi}(x,y;k,\gamma) = \sum_n \frac{f_n}{\left(k^2 - k_n^2 - \gamma^2\right) + 2i\gamma k}\Phi_n(x,y), \tag{18}$$

where the expansion coefficient f_n can be calculated by the overlapping integral as

$$f_n = \iint \Phi_n^*(x,y)\, S(x,y)dxdy. \tag{19}$$

Equation (18) reveals that the resonance generally occurs at the driving wave number k to be fairly close to the eigenvalue k_n. The excitation sources in most resonant systems, including quantum-dot billiards, microwave cavities, microcavity lasers, and optical waveguides [58,59], are usually localized and unidirectional. Therefore, it is practically useful to model the source distribution $S(x,y)$ as a Gaussian wave packet with a specific momentum (p_x,p_y):

$$S(x,y) = \frac{1}{\sigma\sqrt{\pi}}\exp\left(-\frac{(x-x_0)^2}{\sigma^2}\right)\exp\left(-\frac{(y-y_0)^2}{\sigma^2}\right)\exp\left(i\frac{p_x}{\hbar}(x-x_0)\right)\exp\left(i\frac{p_y}{\hbar}(y-y_0)\right), \tag{20}$$

where (x_0,y_0) denotes the central position and σ is the width of the wave packet. It is worthwhile to mention that the Gaussian wave packet has been widely used to study the time evolution of the wave function in quantum billiards [19,20]. The equilateral-triangular billiards is considered to demonstrate the connection between the stationary coherent states and the experimental resonant modes. Substituting Eqs. (2) and (20) into Eq. (19), after some algebra, the response wave function in Eq. (18) can be derived as

$$\tilde{\Psi}^{(\pm)}(x,y;k,\gamma) = \sum_{m,n} A_{m,n}(\tilde{k})\Phi_{m,n}^{(\pm)}(x,y) = \sum_{m,n}\frac{f_{m,n}}{\left(k^2 - k_{m,n}^2 - \gamma^2\right) + 2i\gamma k}\Phi_{m,n}^{(\pm)}(x,y), \tag{21}$$

where

$$\begin{aligned} f_{m,n} = {} & G^{(\pm)}\left(x_0,p_x,\frac{4m-2n}{3}\right)G^{(s)}\left(y_0,p_y,\frac{2n}{\sqrt{3}}\right) - G^{(\pm)}\left(x_0,p_x,\frac{4n-2m}{3}\right)G^{(s)}\left(y_0,p_y,\frac{2m}{\sqrt{3}}\right) \\ & + G^{(\pm)}\left(x_0,p_x,\frac{-2m-2n}{3}\right)G^{(s)}\left(y_0,p_y,\frac{2m-2n}{\sqrt{3}}\right) \end{aligned} \tag{22}$$

and

$$G^{(s)}(\rho,P,\lambda) = \pi^{1/4}\sqrt{\sigma}\exp\left\{-\frac{\sigma^2}{4}\left[\left(\frac{P^2}{\hbar}\right) + \left(\frac{\lambda\pi}{a}\right)^2\right]\right\} i\sinh\left[\left(\frac{\lambda\pi}{a}\right)\left(\frac{\sigma^2 P}{2\hbar} - i\rho\right)\right],$$

$$G^{(c)}(\rho,P,\lambda) = \pi^{1/4}\sqrt{\sigma}\exp\left\{-\frac{\sigma^2}{4}\left[\left(\frac{P^2}{\hbar}\right) + \left(\frac{\lambda\pi}{a}\right)^2\right]\right\} \cosh\left[\left(\frac{\lambda\pi}{a}\right)\left(\frac{\sigma^2 P}{2\hbar} - i\rho\right)\right], \tag{23}$$

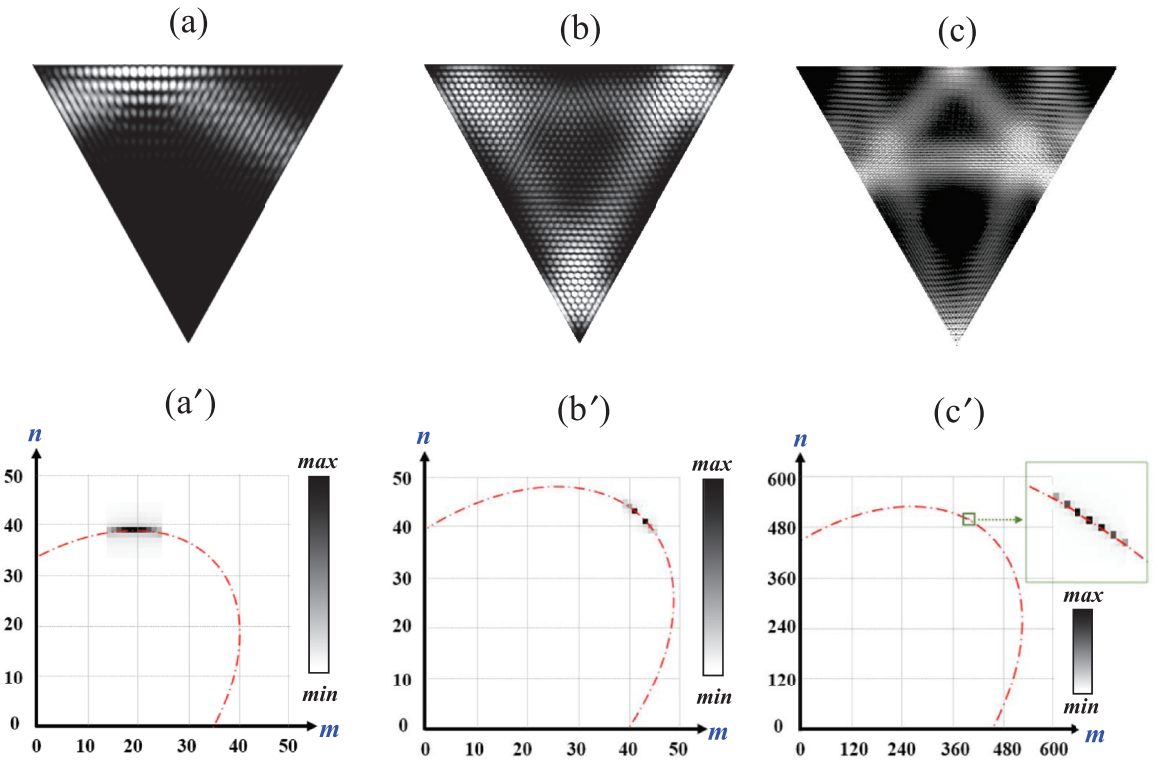

FIG. 10. Wave patterns of $|\tilde{\Psi}^{(\pm)}(x,y;k,\gamma)|$ with different parameters: (a) $(x_0,y_0)=(-0.43a,0.70a)$, $N=20$, and $(p,q)=(1,0)$; (b) $(x_0,y_0)=(-0.45a,0.95a)$, $N=15$, and $(p,q)=(1,1)$; and (c) $(x_0,y_0)=(0,0.577a)$, $N=100$, and $(p,q)=(2,1)$. (a′)–(c′) Absolute values of the weighting coefficient $|A_{m,n}|$ for each resonant mode corresponding to the cases in (a)–(c), respectively.

with $G^{(\pm)}(\rho,P,\lambda)=G^{(c)}(\rho,P,\lambda)\pm iG^{(s)}(\rho,P,\lambda)$. To obtain the response wave function with the intensity maxima localized on the classical PO denoted by (p,q), the momenta of the Gaussian wave packet are set as $p_x=2\hbar\pi(n_0+m_0)/3a$ and $p_y=2\hbar\pi(n_0-m_0)/\sqrt{3}a$, where $m_0=(2q+p)N$ and $n_0=(2p+q)N$, which can be comprehended from Sec. II. The mass of the particle is assumed to be unity for convenience. From Eq. (21) it can be clearly found that the resonant mode at $k=k_{m_0,n_0}$ is mainly dominated by the superposition of the nearly degenerate eigenstates around the central order (m_0,n_0). To be more specific, the condition $k=k_{m_0,n_0}$ in the denominator of the right-hand side of Eq. (21) effectively leads the double summations to be a single summation that is only contributed by the group of nearly degenerate eigenstates $\Phi^{(\pm)}_{m_0+pK,n_0-qK}$, which is the same as the form of the stationary coherent state.

Figures 10 shows the wave patterns of $|\tilde{\Psi}^{(\pm)}(x,y;k,\gamma)|$ for three cases: $(x_0,y_0)=(-0.43a,0.70a)$, $N=20$, and $(p,q)=(1,0)$ [Fig. 10(a)]; $(x_0,y_0)=(-0.45a,0.95a)$, $N=15$, and $(p,q)=(1,1)$ [Fig. 10(b)]; and $(x_0,y_0)=(0,0.577a)$, $N=100$, and $(p,q)=(2,1)$ [Fig. 10(c)]. The width of the Gaussian wave packet and the damping factor are set equal to $\sigma=0.05a$ and $\gamma=0.2a^{-1}$, respectively. The absolute values of the weighting coefficient $|A_{m,n}|$ for three resonant modes are plotted in Figs. 10(a′)–10(c′) to reveal the dominated eigenstates more clearly. It can be seen that the dominated eigenstates in the resonant modes are well distributed on the tangent of the constant energy contour with central order (m_0,n_0). The nearly complete overlap leads the resonant modes to be similar to the stationary coherent states with the intensity maxima perfectly localized on the classical POs.

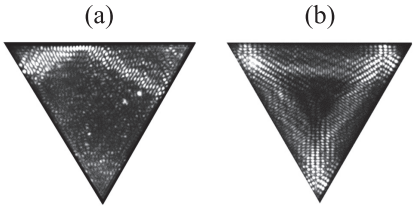

FIG. 11. Wave patterns of the lasing modes observed in a VCSEL with equilateral-triangle transverse confinement.

Finally, the wave patterns of the lasing modes observed in a vertical-cavity surface-emitting laser (VCSEL) with an equilateral-triangle transverse confinement are shown in Figs. 11(a) and 11(b) to further confirm the validity of the proposed theoretical treatments. The device structures and the operation conditions of the equilateral-triangle VCSEL are identical to the case in Ref. [52]. The perfect consistency between the theoretical results in Figs. 10(a) and 10(b) and the experimental wave patterns in Figs. 11(a) and 11(b) provides the feasibility of using the proposed model to analyze the trajectorylike wave functions for further applications such as ballistic transports and directional emissions.

V. CONCLUSION

We have thoroughly demonstrated that the wave patterns of quantum stationary coherent states formed by nearly

degenerate eigenstates are well localized on the classical POs in integrable billiards, including the equilateral-triangular and circular shapes. By using quantum stationary coherent states, a theoretical approach has been developed to extract the trajectory equations for classical POs. The extracted trajectory equations clearly reveal the relationship between the phase factors of quantum stationary coherent states and the initial positions of classical POs. Moreover, we have shown that the stationary coherent states with noncoprime parametric numbers correspond to multiple POs, which has no correspondence in the one-particle picture. We have further verified that the stationary coherent states can be linked to the experimental resonant modes generated by a localized and unidirectional source. It is believed that the excellent agreement between the resonant modes and the stationary coherent states can offer useful insight into the quantum-classical connection in the mesoscopic regime.

ACKNOWLEDGMENT

This work was supported by the Ministry of Science and Technology of Taiwan (Contract No. MOST105-2628-M-009-004).

[1] S. M. Roy and V. Singh, Phys. Rev. D **25**, 3413 (1982).
[2] W. M. Zhang and R. Gilmore, Rev. Mod. Phys. **62**, 867 (1990).
[3] Y. F. Chen and K. F. Huang, J. Phys. A: Math. Gen. **36**, 7751 (2003).
[4] M. Brack and R. K. Bhaduri, *Semiclassical Physics* (Addison-Wesley, Reading, 1997).
[5] Y. F. Chen, K. F. Huang, and Y. P. Lan, Phys. Rev. E **66**, 046215 (2002).
[6] Y. F. Chen and K. F. Huang, Phys. Rev. E **68**, 066207 (2003).
[7] M. A. Doncheski and R. W. Robinett, Ann. Phys. (N.Y.) **299**, 208 (2002).
[8] S. L. Lin, F. Gao, Z. P. Hong, and M. L. Du, Chin. Phys. Lett. **22**, 9 (2005).
[9] C. C. Liu, T. H. Lu, Y. F. Chen, and K. F. Huang, Phys. Rev. E **74**, 046214 (2006).
[10] Y. F. Chen, Y. C. Lin, W. Z. Zhuang, H. C. Liang, K. W. Su, and K. F. Huang, Phys. Rev. A **85**, 043833 (2012).
[11] M. Wright and R. Weaver, *New Directions in Linear Acoustics and Vibration: Quantum Chaos, Random Matrix Theory and Complexity* (Cambridge University Press, Cambridge, 2010).
[12] E. G. Altmann, T. Friedrich, A. E. Motter, H. Kantz, and A. Richter, Phys. Rev. E **77**, 016205 (2008).
[13] E. J. Heller, Phys. Rev. Lett. **53**, 1515 (1984).
[14] S. W. McDonald and A. N. Kaufman, Phys. Rev. Lett. **42**, 1189 (1979).
[15] S. Tomsovic and E. J. Heller, Phys. Rev. Lett. **67**, 664 (1991).
[16] G. M. Zaslavsky, *Chaos in Dynamic Systems* (Harwood, New York, 1985).
[17] M. C. Gutzwiller, *Chaos in Classical and Quantum Mechanics* (Springer, Berlin, 1990).
[18] S. Sridhar and E. J. Heller, Phys. Rev. A **46**, R1728 (1992).
[19] S. Tomsovic and E. J. Heller, Phys. Rev. E **47**, 282 (1993).
[20] S. Tomsovic and E. J. Heller, Phys. Rev. Lett. **70**, 1405 (1993).
[21] M. V. Berry, J. Phys. A: Math. Gen. **10**, 2083 (1977).
[22] P. O'Connor, J. Gehlen, and E. J. Heller, Phys. Rev. Lett. **58**, 1296 (1987).
[23] R. W. Robinett, J. Math. Phys. **40**, 101 (1999).
[24] R. W. Robinett, Phys. Rep. **392**, 1 (2004).
[25] R. W. Robinett, Surf. Rev. Lett. **05**, 519 (1998).
[26] M. A. Doncheski, S. Heppelmann, R. W. Robinett, and D. C. Tussey, Am. J. Phys. **71**, 541 (2003).
[27] D. F. Styer, Am. J. Phys. **69**, 56 (2001).
[28] R. W. Robinett, Am. J. Phys. **65**, 1167 (1997).
[29] R. W. Robinett, Eur. J. Phys. **24**, 231 (2003).
[30] M. C. M. Wright and C. J. Ham, J. Acoust. Soc. Am. **121**, 1865 (2007).
[31] R. W. Robinett, J. Math. Phys. **39**, 278 (1998).
[32] J. Lu, Prog. Nat. Sci. **18**, 927 (2008).
[33] A. Matzkin, Found. Phys. **39**, 903 (2009).
[34] G. Fonte and B. Zerbo, Eur. Phys. J. Plus **127**, 8 (2012).
[35] R. W. Robinett, Am. J. Phys. **67**, 67 (1999).
[36] M. Macek, P. Cejnar, J. Jolie, and S. Heinze, Phys. Rev. C **73**, 014307 (2006).
[37] W.-K. Lee, Am. J. Phys. **50**, 666 (1982).
[38] R. W. Robinett, *Quantum Mechanics: Classical Results, Modern Systems, and Visualized Examples* (Oxford University Press, Oxford, 1997).
[39] A. S. Sachrajda, R. Ketzmerick, C. Gould, Y. Feng, P. J. Kelly, A. Delage, and Z. Wasilewski, Phys. Rev. Lett. **80**, 1948 (1998).
[40] C.-H. Zhang, F. Kassubek, and C. A. Stafford, Phys. Rev. B **68**, 165414 (2003).
[41] A. M. Chang, H. U. Baranger, L. N. Pfeiffer, and K. W. West, Phys. Rev. Lett. **73**, 2111 (1994).
[42] C. Lafargue, M. Lebental, A. Grigis, C. Ulysse, I. Gozhyk, N. Djellali, J. Zyss, and S. Bittner, Phys. Rev. E **90**, 052922 (2014).
[43] M. Lebental, N. Djellali, C. Arnaud, J.-S. Lauret, J. Zyss, R. Dubertrand, C. Schmit, and E. Bogomolny, Phys. Rev. A **76**, 023830 (2007).
[44] H. C. Chang, G. Kioseoglou, E. H. Lee, J. Haetty, M. H. Na, Y. Xuan, H. Luo, A. Petrou, and A. N. Cartwright, Phys. Rev. A **62**, 013816 (2000).
[45] J. Yoon, S.-J. An, K. Kim, J. K. Ku, and O. Kwon, Appl. Opt. **46**, 2969 (2007).
[46] E. Bogomolny, N. Djellali, R. Dubertrand, I. Gozhyk, M. Lebental, C. Schmit, C. Ulysse, and J. Zyss, Phys. Rev. E **83**, 036208 (2011).
[47] I. Braun, G. Ihlein, F. Laeri, J. U. Nöckel, G. Schulz-Ekloff, F. Schüth, U. Vietze, Ö. Weiss, and D. Wöhrle, Appl. Phys. B **70**, 335 (2000).
[48] H.-T. Lee and A. W. Poon, Opt. Lett. **29**, 5 (2004).
[49] C. Li, L. Zhou, S. Zheng, and A. W. Poon, IEEE J. Sel. Top. Quantum Electron. **12**, 1438 (2006).
[50] E. Marchena, S. Shi, and D. Prather, Opt. Express **16**, 16516 (2008).
[51] C. C. Chen, K. W. Su, Y. F. Chen, and K. F. Huang, Opt. Lett. **33**, 509 (2008).
[52] R. C. C. Chen, Y. T. Yu, Y. J. Huang, C. C. Chen, Y. F. Chen, and K. F. Huang, Opt. Lett. **34**, 1810 (2009).

[53] Y.-F. Chen, Y.-T. Yu, Y.-J. Huang, P.-Y. Chiang, K.-W. Su, and K.-F. Huang, Opt. Lett. **35**, 2723 (2010).
[54] Y. F. Chen, Y. T. Yu, P. Y. Chiang, P. H. Tuan, Y. J. Huang, H. C. Liang, and K. F. Huang, Phys. Rev. E **83**, 016208 (2011).
[55] T. Nobis and M. Grundmann, Phys. Rev. A **72**, 063806 (2005).
[56] D. Yu, Y. Chen, B. Lia, X. Chen, M. Zhang, F. Zhao, and S. Ren, Appl. Phys. Lett. **91**, 091116 (2007).
[57] J. Dai, C. X. Xu, K. Zheng, C. G. Lv, and Y. P. Cui, Appl. Phys. Lett. **95**, 241110 (2009).
[58] H.-J. Stöckmann, *Quantum Chaos—An Introduction* (Cambridge University Press, Cambridge, 1999).
[59] P. H. Tuan, C. P. Wen, Y. T. Yu, H. C. Liang, K. F. Huang, and Y. F. Chen, Phys. Rev. E **89**, 022911 (2014).
[60] W.-K. Li and S. M. Blinder, J. Chem. Educ. **64**, 130 (1987).